

Multi-scale classification of disease using structural MRI and wavelet transform

Kerstin Hackmack^{a,b,*}, Friedemann Paul^{c,e}, Martin Weygandt^{a,b,c},
Carsten Allefeld^{a,b}, John-Dylan Haynes^{a,b,c,d,*}
and The Alzheimer's Disease Neuroimaging Initiative¹

^a Bernstein Center for Computational Neuroscience, Charité—Universitätsmedizin Berlin, Berlin, Germany

^b Berlin Center for Advanced Neuroimaging, Charité—Universitätsmedizin Berlin, Berlin, Germany

^c NeuroCure Clinical Research Center, Charité—Universitätsmedizin Berlin, Berlin, Germany

^d Berlin School of Mind and Brain, Humboldt-Universität zu Berlin, Berlin, Germany

^e Experimental and Clinical Research Center, Max Delbrueck Center for Molecular Medicine, Berlin, Germany

ARTICLE INFO

Article history:

Accepted 9 May 2012

Available online 15 May 2012

Keywords:

Multi-scale classification

Multiple sclerosis

Structural MRI

Support vector machine

Wavelet transform

ABSTRACT

Recently, multivariate analysis algorithms have become a popular tool to diagnose neurological diseases based on neuroimaging data. Most studies, however, are biased for one specific scale, namely the scale given by the spatial resolution (i.e. dimension) of the data. In the present study, we propose to use the dual-tree complex wavelet transform to extract information on different spatial scales from structural MRI data and show its relevance for disease classification. Based on the magnitude representation of the complex wavelet coefficients calculated from the MR images, we identified a new class of features taking scale, directionality and potentially local information into account simultaneously. By using a linear support vector machine, these features were shown to discriminate significantly between spatially normalized MR images of 41 patients suffering from multiple sclerosis and 26 healthy controls. Interestingly, the decoding accuracies varied strongly among the different scales and it turned out that scales containing low frequency information were partly superior to scales containing high frequency information. Usually, this type of information is neglected since most decoding studies use only the original scale of the data. In conclusion, our proposed method has not only a high potential to assist in the diagnostic process of multiple sclerosis, but can be applied to other diseases or general decoding problems in structural or functional MRI.

© 2012 Elsevier Inc. All rights reserved.

Introduction

In recent years, multivariate analysis algorithms have become a popular tool to diagnose neurological or psychiatric diseases based on structural or functional MRI data (Ashburner and Klöppel, 2011; Koutsouleris et al., 2009; Weygandt et al., 2011). The main challenge here lies in the identification of features which provide most

Abbreviations: dt-CWT, dual-tree complex wavelet transform; MRI, magnetic resonance imaging; MS, multiple sclerosis; NABT, normal-appearing brain tissue; SVM, support vector machine.

* Corresponding authors at: Bernstein Center for Computational Neuroscience, Charité—Universitätsmedizin Berlin, Haus 6, Philippstr. 13, 10115 Berlin, Germany. Fax: +49 30 209 367 69.

E-mail addresses: kerstin.hackmack@bccn-berlin.de (K. Hackmack), friedemann.paul@charite.de (F. Paul), martin.weygandt@bccn-berlin.de (M. Weygandt), carsten.allefeld@bccn-berlin.de (C. Allefeld), haynes@bccn-berlin.de (J.-D. Haynes).

¹ Data used in the Supplementary material of this article were obtained from the Alzheimer's Disease Neuroimaging Initiative (ADNI) data base (<http://www.loni.ucla.edu/ADNI>). As such, the investigators within the ADNI contributed to the design and implementation of ADNI and/or provided data but did not participate in analysis or writing of this report. The complete list of ADNI investigators can be found here: http://www.loni.ucla.edu/ADNI/Collaboration/ADNI_Authorship_list.pdf.

information about the particular disease (so-called 'disease signatures'). Features used in previous studies include local or global intensity patterns (e.g. Klöppel et al., 2008b; Weygandt et al., 2011) as well as geometric and surface-based features (Ecker et al., 2010; Yotter et al., 2011). Most studies, however, are biased for specific scales, namely the scale given by the spatial resolution of the data. Although it is well known that the brain is hierarchically organized at different spatial scales, ranging from individual neurons over cortical columns to larger functional brain areas, the interplay between these spatial scales has been little addressed. This limitation can partly be overcome by using wavelets which provide a powerful means to analyze the patterning of complex data on different scales (Sajda et al., 2002). By this, wavelets allow "zooming in" at different spatial scales and thus can be interpreted as a form of dimensionality reduction.

A wavelet is a small wave-like oscillation which is used to decompose a signal with respect to scaled and translated versions of it. In contrast to sine waves used as basis functions in the Fourier transform, wavelets are of limited duration and therefore allow for localization in scale and space (Graps, 1995). By this, the wavelet transform provides a natural adaptability to local signal properties and non-stationary signals and thus can be used to analyze oriented discontinuities (i.e. directionality) such as edges or surfaces in the

data (Selesnick et al., 2005). Intuitively, the wavelet transform can be seen as a way of decomposing the energy of a signal into a hierarchically organized set of scales (Bullmore et al., 2004). High frequency components of the energy are represented by wavelet coefficients at fine scales, whereas low frequency components can be found at coarse scales. For an introduction into wavelets, please refer to Daubechies (1992), Graps (1995) or Mallat (2008). The multi-resolution property of the wavelet transform has been used in a variety of applications including functional MRI analysis (for a review see Bullmore et al., 2004 or Van De Ville et al., 2006). In the medical context, wavelets have been used as a way to discriminate between healthy and pathological tissue (e.g. tumor cells or lesions; Antel et al., 2003; Castellano et al., 2004; Zhang et al., 2008). However, these studies were mostly based on 2-dimensional medical images and did not focus on the importance of different spatial scales in distinguishing the tissue classes. Although multi-scale representations of medical data promise a rich source of information for disease classification, we are not aware of any study investigating the impact of different scales in decoding a disease.

One of the most common neurological diseases is multiple sclerosis (MS), which has only barely been investigated within the context of multivariate analysis algorithms. MS is an autoimmune disease that affects the central nervous system leading to inflammation, demyelination and neurodegeneration of brain tissue (Compston and Coles, 2008). These alterations can cause a number of neurological problems such as impaired function of the motor, somatosensory or visual system. Since the introduction of the McDonald criteria (McDonald et al., 2001), conventional MRI has become one of the cornerstones in diagnosing MS. Radiologically, MS is mainly characterized by three neurobiological markers: focal inflammatory lesions, neurodegeneration and subtle tissue alterations (Filippi and Rocca, 2005). In contrast to lesions, regional neurodegeneration and subtle tissue alterations usually remain undetected in conventional MRI and are therefore termed normal-appearing brain tissue (NABT; Filippi et al., 2004). In two recent studies of our group, however, we have shown that local intensity patterns extracted from NABT areas contain information about disease status (Weygandt et al., 2011) and symptom severity (Hackmack et al., 2012). These studies, however, were only based on the original size of the MR volumes and therefore did not cover multi-scale information.

Here, we use wavelets to investigate the significance of *different scales* in discriminating between MR images of MS patients and healthy controls. For the wavelet decomposition, we used the dual-tree complex wavelet transform (Kingsbury, 2001; Selesnick et al., 2005) which has the advantage of being approximately shift-invariant and directionally selective. For 3-dimensional MR volumes, 28 different directions can be isolated. This means that on each scale 28 orientation subbands (which are again 3-dimensional volumes) are generated with each capturing one specific direction in the data. Based on the magnitude of the complex wavelet coefficients in each of the subbands, we used two strategies to investigate directionality at different scales. In the first analysis ('global analysis of anisotropy'), we calculated for each subject the overall energy contained in each of the subbands at one particular scale. This type of features ('global wavelet features') captured scale and directionality information, but disregarded local information by assessing the energy throughout all brain locations. For each scale, it leads to one final diagnosis per subject. In contrast, in the second analysis ('local analysis of anisotropy') we used the local pattern of directionality by including the *position* within the subbands. These features ('local wavelet features') allow for a precise mapping of relevant regions. Both analyses were conducted for each scale separately. To classify between global or local wavelet features of MS patients and healthy controls, we used a linear support vector machine (Cortes and Vapnik, 1995; Shawe-Taylor and Christianini, 2000).

Materials and methods

Patients

We reanalyzed the data of 41 patients (21 females and 20 males; age, median (MD)=34, range 19–51) with clinically definite MS (relapsing-remitting type; McDonald et al., 2001) and 26 age and gender matched healthy controls (14 females, 12 males; age, MD=36.5, range 23–57) already used in two previous studies of our group (Hackmack et al., 2012; Weygandt et al., 2011). Disease duration was on average 84.0 months (standard deviation (SD)=76.3). Mean T1 lesion load was 1872.2 mm³ (SD=6279.5; 'black holes') and T2 lesion load was 5224.0 mm³ (SD=4117.8). The patients exhibited a mild to moderate score on the Expanded Disability Status Scale (EDSS; Kurtzke, 1983; MD=2, range 0–7). Additionally, patients were scored on the Multiple Sclerosis Functional Composite (MSFC; Cutter et al., 1999) and subtests 9-Hole Peg Test (9-HPT; mean (M)=19.4, SD=3.3), Timed Walk Test (TWT; M=5.0, SD=1.7), and Paced Auditory Serial Addition Test (PASAT; M=52.4, SD=9.1). Consent was obtained according to the Declaration of Helsinki, and the study was approved by the research ethics committee of the Charité–Universitätsmedizin Berlin. All subjects gave written informed consent.

Magnetic resonance imaging

Whole-brain high-resolution 3-dimensional T1-weighted images (MPRAGE, TR 2110 ms, TE 4.38 ms, TI 1100 ms, flip angle 15°, resolution 1×1×1 mm) and T2-weighted fluid-attenuated inversion recovery sequence images (TIRM, TR 10000 ms, TE 108 ms, TI 2500 ms, resolution 1×1×3 mm, 44 contiguous axial slices) were acquired using a 1.5 Tesla MRI (Magnetom Sonata, Siemens, Erlangen, Germany) with an 8-channel standard head coil. Lesion load for MPRAGE and TIRM images was routinely measured using the MedX v.3.4.3 software package (Sensor Systems Inc., Sterling, VA, USA). Lesion load of TIRM images was additionally measured using in-house software (Weygandt et al., 2011).

Preprocessing

In accordance with our previous studies (Hackmack et al., 2012; Weygandt et al., 2011), several preprocessing steps were performed. First, a clinician used in-house software to conduct a lesion mapping based on individual TIRM images. To be as conservative as possible, the clinician was instructed to mark any hyperintensities visible in the TIRM images and not only oval lesions as it is common in clinical practice. Next, correction of field inhomogeneities, coregistration of high-resolution MPRAGE and TIRM images, and spatial normalization of these high-resolution images to the Montreal Neurological Institute (MNI) 152 brain template (voxel resolution: 2×2×2 mm) were conducted using SPM5 (Wellcome Trust Centre for Neuroimaging, Institute of Neurology, UCL, London, <http://www.fil.ion.ucl.ac.uk/spm>). The spatial normalization parameters for the MPRAGE images were estimated by the 'unified segmentation approach' (Ashburner and Friston, 2005) and then applied to the co-registered TIRM images as well as to individual lesion masks. Importantly, lesion areas identified by the clinician were excluded to avoid lesion-mediated artifacts in the normalization routine. Finally, we obtained TIRM images from all subjects as well as their individual lesion masks in MNI space (volume size: 79×95×69; voxel size: 2×2×2 mm).

For the wavelet transformation, the spatial normalized TIRM images were masked in three different ways (Fig. 1). First, all voxels within the SPM standard brain mask that were not cerebrospinal fluid (CSF) with a probability of more than 0.8 (based on SPM CSF prior map) were included (referred to as brain mask). The rather conservative threshold of 0.8 was chosen to avoid misinterpretation of tissue-free voxels as brain tissue. Based on the brain mask, we created

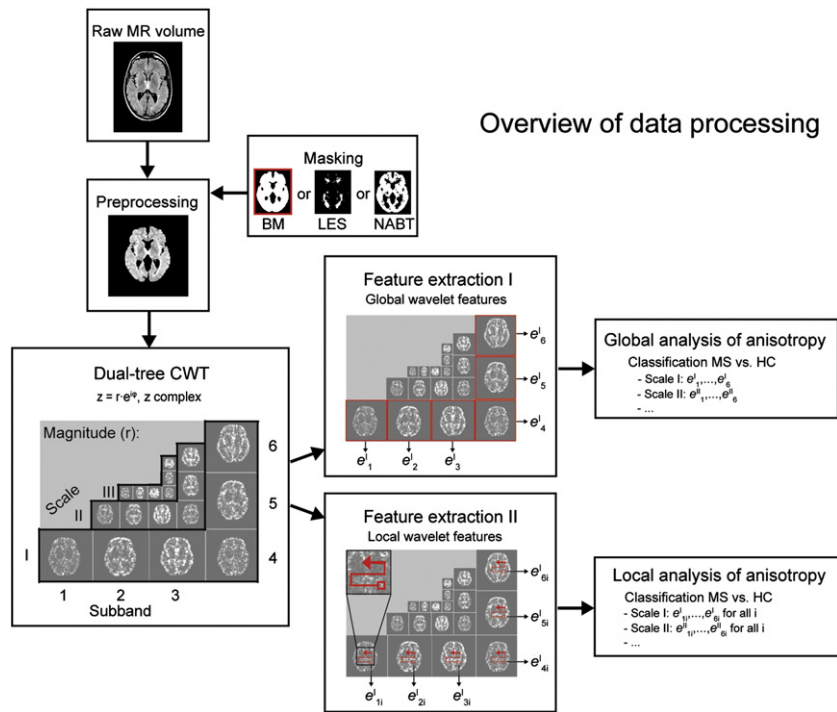


Fig. 1. Overview of data processing. Raw MR volumes were normalized to the Montreal Neurological Institute (MNI) template and then masked by one of the three masks: brain mask (BM), lesion mask (LES) or normal-appearing brain matter mask (NABT). For the resulting MR volumes, we calculated a 6-level dual-tree complex wavelet transform (dt-CWT) resulting in 6 different scales and 28 oriented subbands (see Fig. 2) per scale, where each subband is again a 3-dimensional volume containing a different number of voxels depending on scale. For illustration, we here show an example of a 3-level dt-CWT of a 2-dimensional MR image resulting in 3 scales and 6 subbands per scale. Each subband isolates a specific direction in the image ($\pm 15^\circ$, $\pm 45^\circ$, $\pm 75^\circ$). Based on the magnitude representation of the wavelet coefficients, we extracted either global wavelet features (feature extraction I) or local wavelet features (feature extraction II). For the global wavelet features, we calculated the log-energy for each subband within a particular scale (Figure: Scale I). Please note that the log-energy is computed *across* all positions within a subband. We then conducted a classification analysis ('global analysis of anisotropy') for each scale separately to discriminate between the features of MS patients (MS) and healthy controls (HC). For the local wavelet features, we extracted the magnitude at one particular location (i.e. voxel position) across all subbands within one scale. Thus, the features depend not only on the scale but also on the position within the subband and therefore represent *local* directional information. The features were then used as above by a classification analysis ('local analysis of anisotropy') to separate between the two groups. Importantly, the classification analysis was not only conducted separately for each scale, but also for each voxel position.

two further masks: (1) lesion mask and (2) normal-appearing brain matter (NABT) mask. Whereas the lesion mask includes only that matter where at least one person had a lesion, the NABT mask includes only that matter where *none* of the MS patients had a lesion. Please note that within the lesion mask only 6.83% of voxels across all subjects were actually lesioned. The lesion and NABT mask together add up to the brain mask. Only image intensity values within the mask (brain, lesion or NABT) were used for calculating the wavelet coefficients, all other values were set to zero. Since the masks were equal for MS patients and healthy controls, boundary effects introduced in the decomposition due to prior masking are equal for both groups and are therefore not relevant for classification. In Supplementary Table 1, results without prior masking are depicted, which show significant results for scales I, III and all scales together. To account for different overall intensity levels the images were standardized within subjects by subtracting the mean and dividing by the standard deviation of normal-appearing (i.e. non-lesional) brain tissue. This was done to ensure that a higher lesion load did not introduce any biases into the standardization. Since the wavelet implementation requires the image dimensions to be a power of 2, we filled the MR volumes with zeros until the next power of 2 is achieved (new volume size: $128 \times 128 \times 128$).

To rule out that the results obtained for the discrimination of MS patients and healthy controls relied on effects related to MS-related preprocessing steps (i.e. lesion masking), we repeated the global and local analyses of anisotropy for an MRI data set of 20 Alzheimer's patients and 20 healthy controls obtained from the Alzheimer's Disease Neuroimaging Initiative (ADNI) data base (see Supplementary material and Supplementary Tables 7–8).

Wavelet decomposition

The discrete wavelet transform (DWT; Burrus et al., 1997; Daubechies, 1992; Graps, 1995; Mallat, 1989, 2008) is a powerful tool to handle signals at different scales. Within the DWT, a signal is broken up into shifted and scaled versions of one original 'mother-wavelet'. For 2- or 3-dimensional signals, this mother-wavelet is a spatial pattern and is usually required to have compact support and vanishing higher moments (Daubechies, 1988, 1992; Meyer, 1987). As a consequence of limited duration, wavelets allow for localization in scale (i.e. frequency) *and* space and can therefore be used to analyze local, spatial transients in the data such as edges or surfaces (Bullmore et al., 2004; Selesnick et al., 2005). This means that wavelets allow capturing information at different spatial scales while maintaining locality. By this, the wavelet transform provides a huge advantage over the Fourier transform, which is only localized in frequency and thus cannot be used to analyze local patterns. Intuitively, the DWT allows for zooming in at particular scales of interest. Since the spatial resolution of the signal is reduced in each decomposition step, the wavelet transform is also a form of dimensionality reduction. In this respect, the DWT can be viewed as a way to decompose the energy of a signal over a hierarchy of scales distributed to different directions in the data (Bullmore et al., 2004). Computationally, the DWT can be implemented via a filter bank (Burrus et al., 1997), which provides a fast way to calculate the wavelet coefficients by using an array of high and low pass filters.

The dual-tree complex wavelet transform (dt-CWT; Kingsbury, 2001; Selesnick et al., 2005; MATLAB implementation can be found here: <http://taco.poly.edu/WaveletSoftware/>) is an improvement of

the DWT, which calculates the complex transform of a signal using two real DWTs. The dt-CWT can then be represented by the matrix $F = [F_h \ F_g]$, where the matrices F_h and F_g represent the real transforms. The complex wavelet coefficients of a real signal x are then given by $F_h \cdot x + i \cdot F_g \cdot x$. Thus, the first DWT gives the real part of the transform, and the second DWT the imaginary part. Both DWTs are implemented via a filter bank, but use different sets of filters. However, the filters are jointly designed to ensure that the overall transform is approximately analytic (Selesnick et al., 2005). By this, the dt-CWT provides two main advantages over the standard DWT: approximate shift-invariance and high direction selectivity in two and higher dimensions.

Shift-invariance means that the wavelet coefficients do not change when the signal is shifted in the time or space domain. Approximate shift-invariance, however, is realized at the cost of a redundancy of 2^d wavelet coefficients (d dimension; i.e. 8-times as many coefficients are needed to represent a 3-dimensional MR image in the dual-tree wavelet domain).

Direction selectivity allows for an isolation of different directions in the signal, for example edges in images or surfaces in volumes. For a 2-dimensional image, 6 different directions can be isolated ($\pm 15^\circ$, $\pm 45^\circ$, $\pm 75^\circ$; Fig. 1), whereas for a 3-dimensional volume, 28 different orientations can be segregated (Fig. 2). Importantly, these orientations are present at each spatial scale. Please note that the standard DWT can only distinguish between horizontal and vertical directions, but not between diagonal directions (so-called ‘checkboard artifact’). In Supplementary Fig. 1, Fourier transform,

standard DWT and dt-CWT are compared with respect to their effect on a 2-dimensional image.

For each subject, we calculated a 6-level dt-CWT based on the preprocessed 3-dimensional MR volumes resulting in 6 different scales (from scales I to VI, VI describing the coarsest) and 28 oriented subbands per scale. These subbands are again 3-dimensional volumes, which contain a certain number of voxels depending on the scale. The number of voxels refers to the spatial resolution of the particular scale. In our case, the 28 orientation subbands at the first scale have a resolution of $64 \times 64 \times 64$, the orientation subbands at the second scale have a resolution of $32 \times 32 \times 32$ and so on. Each voxel within a subband is described by a complex wavelet coefficient which is provided by the dt-CWT. Here, we use the magnitude representation of the complex wavelet coefficients since we are interested in directionality at different scales and the relative magnitude can be seen as a marker of directionality: a larger magnitude indicates the presence of structures of a particular scale and orientation in the data (e.g. edges or surfaces). Consequently, the magnitude of each voxel depends on the scale, the orientation and the position of the voxel within the subband. Please note that the voxel size differs between the different spatial scales and thus the term voxel is not restricted to the voxels in the raw MRI data but is generally meant for ‘volume element’ (where the size is determined by the scale).

For decomposition, we used the Kingsbury Q-filters which are an improved version of the original dt-CWT filters that have better orthogonality and symmetry properties (Kingsbury, 2000). As mentioned

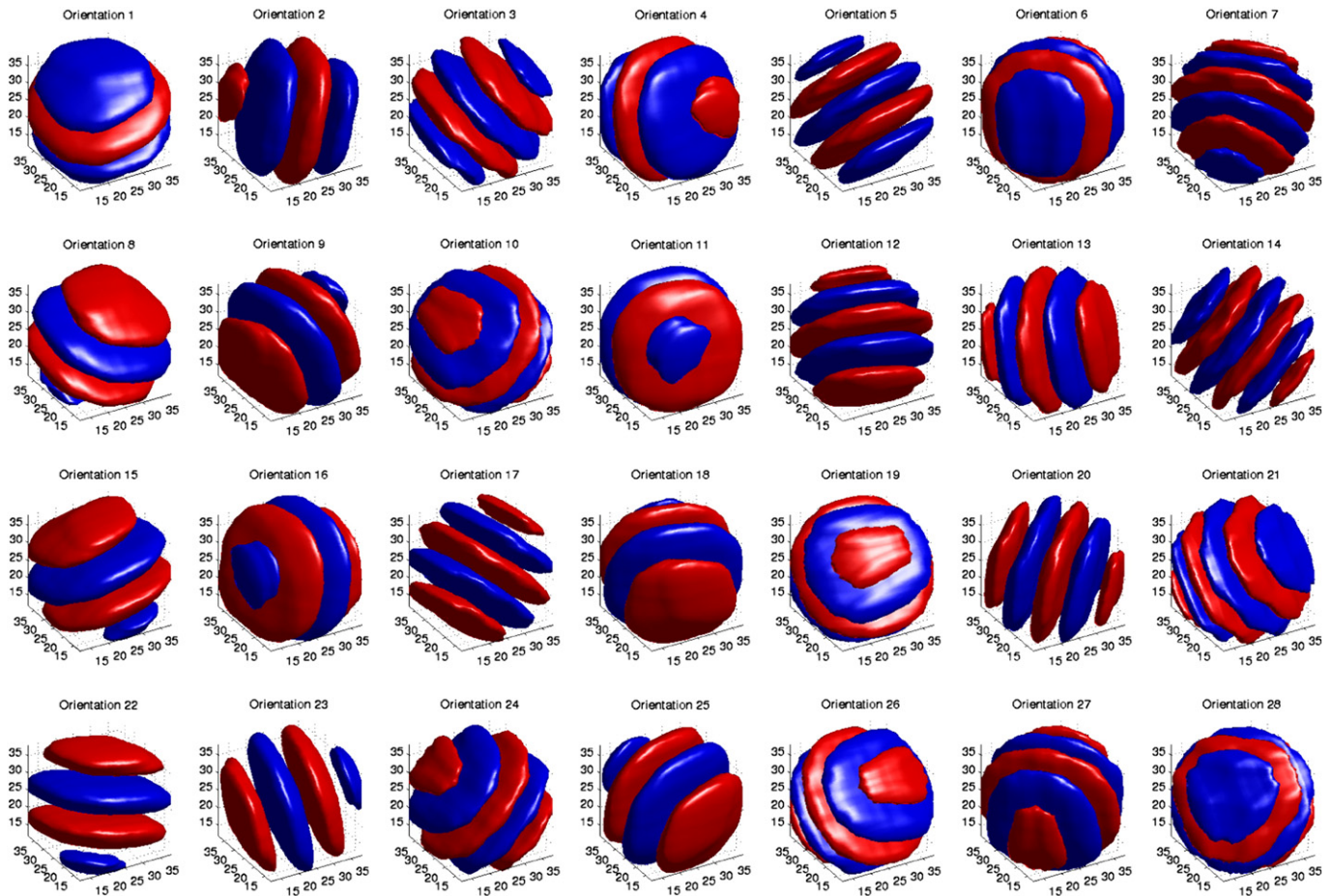


Fig. 2. 3-dimensional isosurfaces. The real part of the complex isosurfaces given by the dual-tree complex wavelet transform is shown for each subband, where each subband corresponds to a specific orientation. These illustrations were made with the same software we used for calculating the dual-tree complex wavelet transform (<http://taco.poly.edu/WaveletSoftware/>).

above, the dt-CWT was calculated three times for each subject, once for each of the three masks (i.e. brain mask, lesion mask and NABT mask), so that either intensity values within all brain matter or lesion matter or NABT contributed to the wavelet coefficients.

Based on the magnitude representation and for each scale separately, we used two strategies to extract features from the wavelet decomposition that are explained in detail in the following sections. The first strategy was to extract patterns of *global* directionality contained in the individual wavelet decompositions ('global wavelet features'), whereas the second strategy was to extract patterns of *local* directionality ('local wavelet features'). Whereas the global features were defined as the total variance in each of the subbands at one particular scale and thus capture scale and directionality information, the local features additionally captured local information by including the position within the subbands. These features were then used independently to classify between MS patients and healthy controls. The analysis based on the global wavelet features is called 'global analysis of anisotropy', whereas the analysis based on the local wavelet features is called 'local analysis of anisotropy'.

Anisotropy generally refers to the property of being directionally dependent, as opposed to isotropy, which means uniformity in all directions. Here, anisotropy deals with the individual pattern of global or local directionality, i.e. how large variance or magnitude measures are in certain directions. The idea here is to find group-specific differences in directionality at different scales. For example, patients may have larger variances in more horizontal directions at one particular scale and may have reduced variances at another scale, whereas healthy subjects show a vice-versa relationship with respect to vertical directions.

Global analysis of anisotropy

As described above, the preprocessed 3-dimensional MR volumes of all MS patients and healthy controls were independently wavelet transformed into a set of volumes at 6 different scales. Each set of volumes consists of 28 orientation subbands isolating certain directions in the data. Each voxel within the orientation subbands is described by the local magnitude value of the wavelet transform. The global analysis of anisotropy now measures variability throughout the brain reflecting potential pathological processes that increase variability in tissue intensity over the whole-brain, e.g. lesions or atrophy. Here, the variability depends on the scale and orientation the data is looked at, but not on the location of a particular tissue alteration.

Specifically, we calculated for each subject the energy contained in each orientation subband across all positions (resulting in 28 values per scale and subject, thus $6 \text{ (scales)} \times 28 \text{ (subbands)} = 168$ values per subject; Fig. 1). Here, energy is defined as the variance of the wavelet transformed MR volumes, decomposed into contributions from different scales and orientations (Selesnick et al., 2005). For each scale separately, the log-energy across subbands (e^S_1, \dots, e^S_{28} , S scale) was used to define feature vectors describing the individual pattern of global directionality. Each value within the feature vector reflects the individual log-energy at a specific combination of scale and orientation (e^{IV}_1 , for example, reflects the log-energy contained in orientation subband 1 of scale IV). Please note that local and thus positional information is lost since we calculated the energy over all magnitude values within the single orientation subbands, so we get one value per orientation subband and subject.

These features were then used by a linear support vector machine (SVM; Cortes and Vapnik, 1995; Shawe-Taylor and Christianini, 2000; Fig. 3) to classify between MS patients and healthy controls. Recently, SVMs have been successfully applied in the field of clinical neuroimaging in order to differentiate two clinical groups (Fu et al., 2008; Klöppel et al., 2008b; Koutsouleris et al., 2009). For an introduction into SVMs, see Burges (1998) or Schölkopf and Smola (2002). Although non-linear kernels are often associated with an improvement in accuracy,

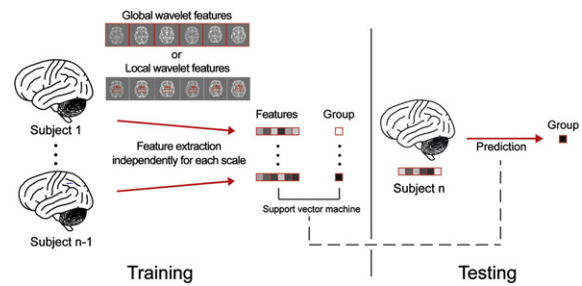


Fig. 3. Illustration of pattern-based classification analysis. In the training phase, global or local wavelet features were extracted from the individual wavelet decompositions of normalized TIRM images. A linear support vector machine (SVM) is then used to classify between MS patients and healthy controls based on the features from the training data set. In the testing phase, global or local wavelet features of a new 'unseen' subject are represented and the SVM is used to predict group membership (MS or healthy control) for this person. For validation, we performed a leave-one-out cross-validation over all subjects, which means that each subject is once the test subject. For the global wavelet features, the whole procedure is repeated for each scale. For the local wavelet features, the procedure is additionally repeated for each voxel position within a particular scale.

we decided here to use a linear SVM since linear classification algorithms have been shown to be most successful in neuroimaging (Mur et al., 2009). Moreover, results obtained from a linear classification algorithm have a clearer and more intuitive interpretation. Nevertheless, results for the naive Bayes classifier and non-linear SVMs are provided in Supplementary Tables 2–4. To perform the classification analyses, we used the LIBSVM toolbox for MATLAB (Chang and Lin, 2011; <http://www.csie.ntu.edu.tw/~cjlin/libsvm/>) with a cost parameter of $C = 1$ (default value). For each set of wavelet coefficients (obtained from either total brain matter, lesion matter or NABT), we conducted a total of 7 classification analyses, one for each scale and one using the features of all scales together. Please note that we were mostly interested in the significance of different scales in decoding MS rather than assessing the performance using the information of all scales together. Therefore, we decided to carry out independent classification analyses for each scale using only the information of this particular scale instead of considering the weight distribution over all scales.

To assess the generalizability of performance using an independent data set, we performed a leave-one-out cross-validation. This means that the feature vectors of all but one subject were used as 'training data'. Based on this training data, the SVM learns a linear function of feature vectors that discriminates between members of two different classes (MS vs. non-MS). This decision function is then tested on the remaining, independent 'test' subject. This procedure was repeated so that each subject was the test subject once. The decoding accuracy is then given by the mean of sensitivity and specificity, where sensitivity (specificity) is defined as the percentage of correctly classified MS patients (healthy controls). A high decoding accuracy implies that the pattern of global directionality spatially encodes information about disease status. Corresponding p-values were calculated using the Pearson's χ^2 test, which tests the null hypothesis of independence between predicted and true class labels.

Local analysis of anisotropy

For the local analysis of anisotropy, the preprocessed 3-dimensional MR volumes of all MS patients and healthy controls were independently wavelet transformed into a set of 28 orientation subbands at 6 different scales containing the magnitude values for each voxel position. This has been done in the same way as for the global analysis of anisotropy. Please recall that voxel refers to 'volume element' and that the size depends on the scale. In contrast to the global analysis of anisotropy, we focused here on particular positions within the brain to allow for finding location-specific alterations in the brain, e.g. subtle tissue alterations at

a particular position that are in most patients present, but not in healthy controls.

Specifically, we used the voxel-wise magnitude values instead of a global variance marker for discriminating between MS patients and healthy controls. Thus, we extracted the magnitude value at the same location (i.e. same voxel position) across all 28 subbands for one particular scale (Fig. 1). The feature vectors therefore depend not only on scale but also on the voxel position ($e^S_{1i}, \dots, e^S_{28i}$, S scale, voxel i) and can be interpreted as the ‘signal energy’ contained in a specific combination of scale, orientation and location (Selesnick et al., 2005). This means that our algorithm searches across the subbands at one particular scale for local directionality patterns informative about the clinical status

Based on the feature vectors, we conducted again a linear SVM to classify between MS patients and healthy controls (Fig. 3). As above, results were validated using a leave-one-out cross-validation and corresponding p-values were calculated using the Pearson’s χ^2 test, which tests the null hypothesis of independence between predicted and true class labels. Please note that the number of voxels and thus the number of classification analyses varied between the three brain matter types and the different scales (i.e. up to 64^3 analyses for scale I, up to 32^3 analyses for scale II and so on). Voxels having zero magnitude were excluded. The high number of classification analyses makes it necessary to correct for multiple comparisons, a statistical problem originating from the fact that if a statistical test is often repeated, it is likely to observe some false positives. To account for the multiple comparison problem in this study, we report only voxel coordinates that exhibit a significant decoding accuracy on a Bonferroni-corrected level of $p < 0.05$, which means that the significance level of 0.05 was divided by the number of classification analyses for either total brain matter, lesion matter or NABT. For example, only voxel coordinates with

$p < 0.05/57508$ (equivalent to $p < 0.05$, Bonferroni corrected) are reported for brain matter. This rather conservative threshold was chosen to increase the specificity of the analyses. Other correction methods commonly used in the neuroimaging literature are false discovery rate control, family wise error correction and permutation testing (Nichols and Hayasaka, 2003). By not reducing the search space prior to the analysis, this approach allows for an unbiased whole-brain information mapping.

Results

Global analysis of anisotropy

For the global analysis of anisotropy, the difference between mean feature vectors of MS patients and healthy controls, respectively, is plotted in Fig. 4A, separately for total brain matter, lesion matter and NABT. Interestingly, their difference varied with respect to scale and orientation. For most subbands and especially for total brain matter and lesion matter, the MS patients tend to have higher energy values. Geometrically, this means that the MR volumes of the patients are characterized by more variability or ‘roughness’ (e.g. caused by the hyperintensity of lesions) than the MR volumes of the controls. For NABT, however, also some negative peaks, where MS patients have lower energy values, could be identified. As expected, the differences were most apparent for lesion matter. Correspondingly, decoding accuracies were largest for lesion matter and varied here between 81.85% and 97.56% with a peak in scale II. For total brain matter, decoding accuracies ranged from 75.56% to 83.07% with a peak in scale III. The differences between the scales were not as strong as for the lesion matter, though. For NABT, the decoding accuracies were smaller, but still significant for scales I, III, IV, V and all scales

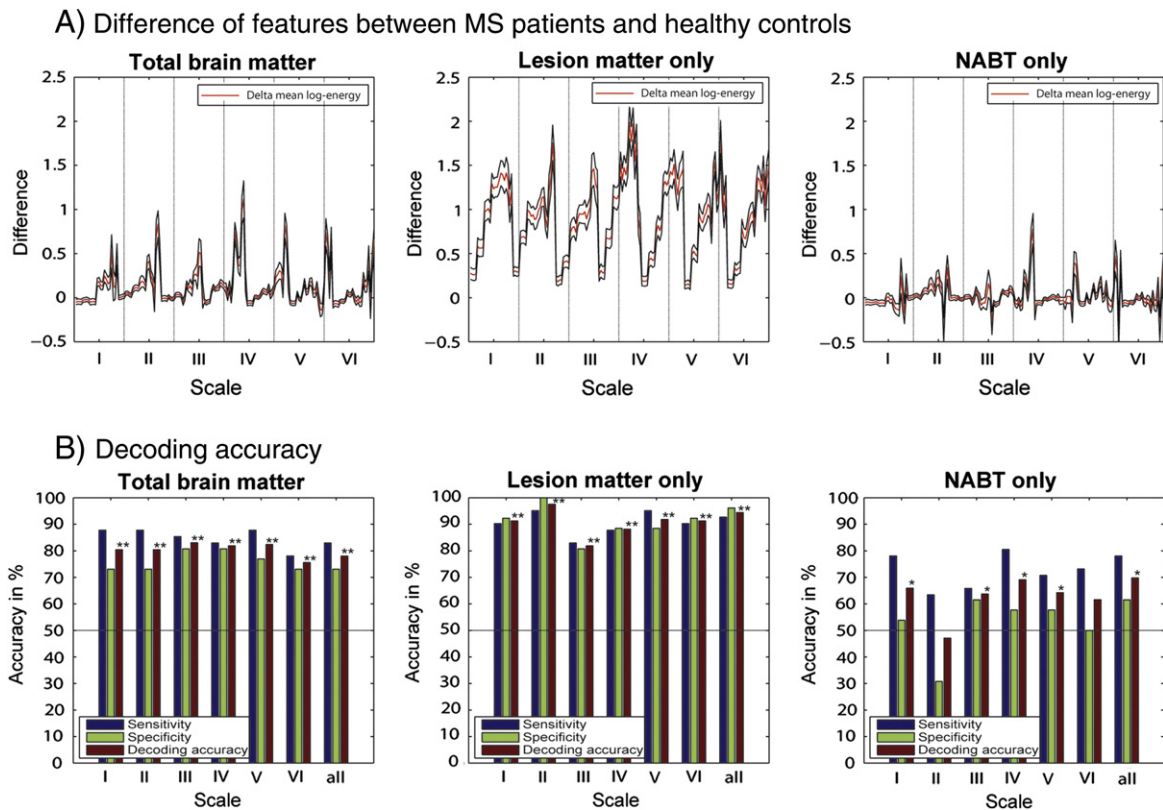


Fig. 4. Results of the global analysis of anisotropy. In (A) the difference of mean feature vectors between MS patients and healthy controls (red) and the standard error (black) is shown for total brain matter, lesion matter and normal-appearing brain matter (NABT), respectively. For each scale, the difference of mean log-energy of all 28 subbands is shown. Sensitivity, specificity and decoding accuracy of corresponding classification analyses are given in (B), separately for each scale and once for all scales together. Significant decoding accuracies are marked by one or two stars (*: $p < 0.05$; **: $p < 0.001$).

Table 1
Results of the global analysis of anisotropy.

	Sensitivity (%)	Specificity (%)	Accuracy (%)	p-value
<i>Scale I</i>				
Brain matter	87.80	73.08	80.44	$<10^{-6}$
Lesions only	90.24	92.31	91.28	$<10^{-10}$
NABT only	78.05	53.85	65.95	0.0074
<i>Scale II</i>				
Brain matter	87.80	73.08	80.44	$<10^{-6}$
Lesions only	95.12	100.00	97.56	$<10^{-13}$
NABT only	63.41	30.77	47.09	0.6251
<i>Scale III</i>				
Brain matter	85.37	80.77	83.07	$<10^{-7}$
Lesions only	82.93	80.77	81.85	$<10^{-6}$
NABT only	65.85	61.54	63.70	0.0280
<i>Scale IV</i>				
Brain matter	82.93	80.77	81.85	$<10^{-6}$
Lesions only	87.80	88.46	88.13	$<10^{-9}$
NABT only	80.49	57.69	69.09	0.0013
<i>Scale V</i>				
Brain matter	87.80	76.92	82.36	$<10^{-7}$
Lesions only	95.12	88.46	91.79	$<10^{-11}$
NABT only	70.73	57.69	64.21	0.0208
<i>Scale VI</i>				
Brain matter	78.05	73.08	75.56	$<10^{-4}$
Lesions only	90.24	92.31	91.28	$<10^{-10}$
NABT only	73.17	50.00	61.59	0.0539
<i>All scales</i>				
Brain matter	82.93	73.08	78.00	$<10^{-5}$
Lesions only	92.68	96.15	94.42	$<10^{-12}$
NABT only	78.05	61.54	69.79	0.0011

NABT, normal-appearing brain tissue. Accuracy is defined as the mean of sensitivity and specificity. Corresponding p-values are calculated using the Pearson's χ^2 test, which tests the null hypothesis of independence between true and predicted class labels.

together. Here, accuracies varied between 47.09% and 69.79% and were largest for scale IV and all scales together. Decoding results including sensitivity, specificity and decoding accuracy are shown in Fig. 4B; corresponding p-values are additionally listed in Table 1. When using the naïve Bayes classifier or non-linear SVMs for classification between MS patients and controls, the decoding results are predominantly worse (Supplementary Tables 2–4), but still significant for total brain matter and lesion matter. This suggests that the classifier uses information from the interaction of different features. Similarly, classification results based on individual log-energy values extracted from spatial normalized MR images without performing a wavelet transform beforehand are inferior to results based on the log-energy extracted from wavelet-transformed MR images (Supplementary Table 5). To address the question whether classification depends on lesion load, we performed a correlation analysis between classifier performance given by individual decision values and lesion load. This analysis revealed that for most scales within the different brain matter types, classifier performance and lesion load were uncorrelated (Supplementary Table 6).

Local analysis of anisotropy

For the local analysis of anisotropy, significant voxels have been found for all three brain matter types and are shown in Fig. 5. In accordance with the global analysis, lesion matter was best in discriminating between MS patients and healthy controls. In particular, most significant voxels were detected for lesion matter ($n = 522$) as

compared to total brain matter ($n = 116$) and NABT ($n = 92$) respectively. Similarly, maximal decoding accuracy was higher for lesion matter (98.78%) than for total brain matter (93.20%) and NABT (92.50%).

As for the global analysis, the performance of classification analyses differed not only between brain matter types, but also for the different scales. For total brain matter, most significant voxels have been found in scales I, II and IV. In comparison, for lesion matter most significant voxels were found for scales III and IV, whereas scales I and II provided most significant voxels for NABT. Please refer to Table 2 for the number of significant voxels since Fig. 5 reflects only a small portion of significant voxels for the low scales.

Interestingly, the proportion of significant voxels steadily increased with scale number, at least for total brain matter and lesion matter. For brain matter, the proportion increased from 0.08% in scale I up to 37.50% in scale VI, whereas for lesion matter even the maximum of 100% was reached for scale VI. For NABT, the proportion increased within scales I and II, dropped at scale III and then again increased. For scale V, a peak of 1.56% was achieved. Please note that for scales IV, V and VI only one or zero significant voxels have been found in the case of NABT. See Table 2 for details.

The general trend to more significant voxels with increasing scale number is also reflected in the histogram of all decoding accuracies (Fig. 6). For higher scales, the whole histogram was shifted to the right and thus contained higher decoding accuracies. For NABT, however, this effect was not as strong as for total brain matter and lesion matter.

Discussion

In the present study, we introduced a novel approach to analyze the patterning of structural MR images at different scales, and its importance for disease classification. In particular, features comprising global or local patterns of directionality at a given scale were shown to discriminate above chance between MS patients and healthy controls. It turned out that scales containing low frequency information were partly superior to scales containing high frequency information.

Two analyses were conducted to investigate the significance of different scales in distinguishing between MS patients and healthy controls. In the global analysis of anisotropy, we have found that even global markers of directionality contain disease-relevant information and allow for significant decoding accuracies with up to 83.07% (scale III) in brain matter, 97.56% (scale II) in lesion matter and 69.79% (all scales together) in normal-appearing brain tissue (NABT). A correlation analysis between classifier performance and lesion load revealed that lesion load was of minor importance for discriminating MS patients and healthy controls. Therefore, the higher variability in MR images of MS patients cannot only rely on the existence of lesions and might be caused by subtle tissue alterations as for example given by atrophy or diffuse white matter abnormalities (i.e. dirty-appearing white matter or micro-lesions, which are too small to be recognized as lesions by a clinician). To the best of our knowledge, this is the first study using global information (covering the whole scope of the brain) for diagnosing MS. In a previous study of our group (Weygandt et al., 2011), we focused on disease-relevant information contained in local spherical patterns (i.e. searchlights) extracted from the MR volumes and therefore we got as many diagnoses as local patterns were investigated. Most other studies focused on the discrimination between lesion areas and normal-appearing white matter (Loizou et al., 2011; Zhang et al., 2008).

In the local analysis of anisotropy, we additionally included local information to obtain a mapping of relevant regions. For single voxel positions, we obtained very high accuracies, not only for brain matter (93.20%) and lesion matter (98.78%), but also for NABT (92.50%). For all three brain matter types, a high number of voxels discriminating significantly between MS patients and healthy

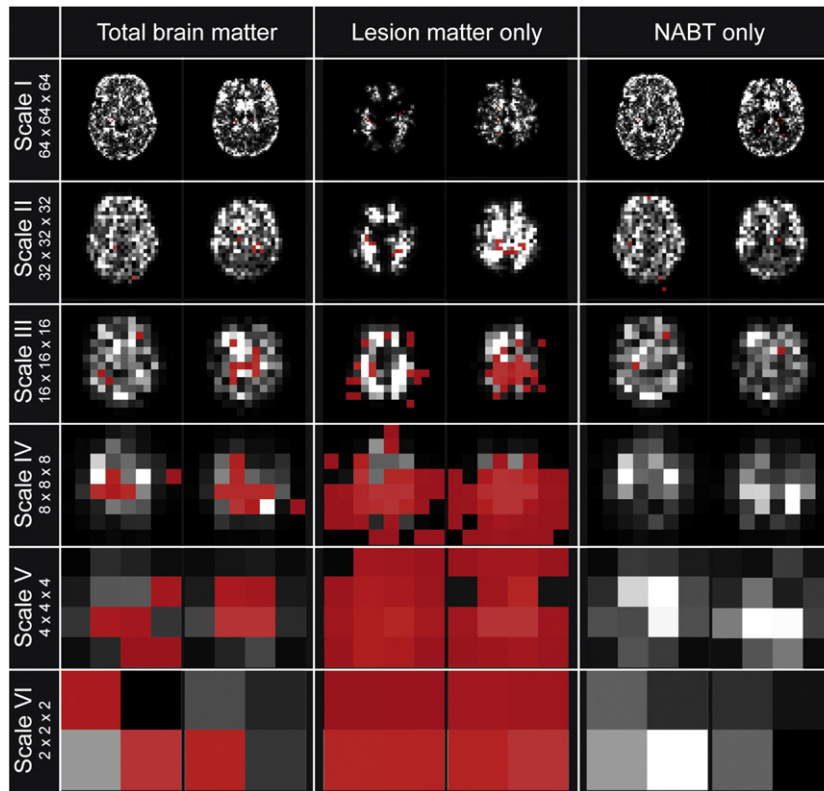


Fig. 5. Results of the local analysis of anisotropy I. Significant voxels (red) are overlaid on a single subject's wavelet decomposition. As described in the [Materials and methods](#) section, the wavelet decomposition was done separately for total brain matter, lesion matter and normal-appearing brain matter (NABT). Please note that the wavelet coefficients are not necessarily zero 'outside' the brain structure and thus allow for significant decoding accuracies there. This is caused by a general "smearing" (reduced spatial resolution, depending on scale) implicit in the wavelet decomposition. Based on the upsampled single subject's wavelet decomposition and the upsampled decoding accuracy map (new size: $128 \times 128 \times 128$), two slices were selected in the same way for all scales and the three brain matter types (slice numbers 52 and 68). However, please note that with increasing scale the number of equal upsampled slices increases (e.g. for scale VI slices from 1 to 64 and slices from 65 to 128 are equal). Please also reconsider that the number of significant voxels indicated in red do not reflect the total number of significant voxels (e.g. for scale I 62 more slices exist with potentially significant voxels). For the exact numbers please refer to [Table 2](#).

controls have been found (116 for total brain matter, 522 for lesion matter and 92 for NABT). Interestingly, the amount of disease-relevant information increased with scale which demonstrates a major importance of low frequency information in decoding MS. A similar result has been found by [Zhang et al. \(2009\)](#). By using the Stockwell transform, they have shown that low frequency information can be a useful means to quantify lesion injury and recovery in MS. In an animal model of MS, [Zhang et al. \(2006\)](#) have additionally shown that frequency information can be directly related to histopathological changes in lesions.

As expected, classifier performance was best for lesion matter, for both global and local analyses of anisotropy. Radiologically, focal inflammatory lesions are the main characteristic of MS pathology ([Filippi and Rocca, 2005](#)) and thus a major involvement of lesions in discriminating MS patients and healthy controls was expected. However, please reconsider that only 6.83% of lesion matter voxels in the lesion mask were actually lesioned, since a voxel was included if it was lesioned in *anyone* patient's brain. Thus, the classifier performance cannot rely on the presence of lesions alone. We hypothesize that the classifier used slight intensity changes due to so-called dirty-appearing white matter, whose importance has recently been highlighted ([Filippi and Rocca, 2010](#); [Ge et al., 2003](#); [Vrenken et al., 2010](#)).

When the classification exclusively relied on NABT, we still obtained very high decoding accuracies for the local analysis. This is in accordance with two earlier studies of our group, which were based on the same data and stated that NABT in conventional MRI

contains substantial disease-relevant information ([Hackmack et al., 2012](#); [Weygandt et al., 2011](#)). This is in contrast to the traditional disregardment of the information value of NABT based on conventional MRI ([Filippi and Rocca, 2005](#)).

In the last years, much effort has been put into finding structural differences in MRI scans between patients suffering from a neurological or psychiatric disease and healthy controls. Features described in the literature include for example intensity values ([Weygandt et al., 2011](#)), grey matter density ([Davatzikos et al., 2008](#); [Draganski et al., 2010](#); [Klöppel et al., 2008b, 2009](#); [Koutsouleris et al., 2009](#)), cortical thickness ([Du et al., 2007](#); [Oliveira et al., 2010](#); [Sailer et al., 2003](#); [Sowell et al., 2008](#); [Worbe et al., 2010](#)), and cortical gyrification ([Ecker et al., 2010](#); [Yotter et al., 2011](#)). Studies using these features mostly differed with respect to the spatial extent of the features. Generally, one can distinguish between voxel-wise analysis, regions-of-interest (ROI) analysis and whole-brain analysis. Conventionally, brain maps have been compared on a voxel-by-voxel basis such as in voxel-based morphometry or in most functional MRI studies ([Ashburner and Friston, 2000](#); [Morgen et al., 2007](#); [Pujol et al., 2004](#)). However, techniques using multivariate information have been demonstrated to be more sensitive than univariate methods in detecting different mental states or diseases ([Ashburner and Klöppel, 2011](#); [Haynes and Rees, 2006](#)). Whereas studies using the whole-brain pattern of features are most suitable for diseases affecting the central nervous system globally such as Alzheimer's disease, ROI analyses are more appropriate for locally acting diseases. In the standard ROI analysis, one or several ROIs are defined in advance

Table 2
Results of the local analysis of anisotropy.

	Max. accuracy (%)	P-value	Bonf. sign. voxel (#)	Proportion (%)
<i>Scale I</i>				
Brain matter	91.79	$<10^{-11}$	36	0.08
Lesions only	91.98	$<10^{-10}$	52	0.21
NABT only	86.21	$<10^{-8}$	53	0.12
<i>Scale II</i>				
Brain matter	88.65	$<10^{-9}$	25	0.23
Lesions only	93.20	$<10^{-11}$	64	0.77
NABT only	92.50	$<10^{-11}$	32	0.29
<i>Scale III</i>				
Brain matter	93.20	$<10^{-11}$	16	0.46
Lesions only	96.34	$<10^{-13}$	138	4.42
NABT only	82.55	$<10^{-6}$	5	0.14
<i>Scale IV</i>				
Brain matter	91.28	$<10^{-10}$	24	4.69
Lesions only	96.86	$<10^{-13}$	203	39.65
NABT only	81.14	$<10^{-6}$	1	0.20
<i>Scale V</i>				
Brain matter	87.43	$<10^{-9}$	12	18.75
Lesions only	98.78	$<10^{-14}$	57	89.06
NABT only	80.44	$<10^{-6}$	1	1.56
<i>Scale VI</i>				
Brain matter	90.57	$<10^{-10}$	3	37.50
Lesions only	91.28	$<10^{-10}$	8	100.00
NABT only	–	–	0	0.00

For each scale, peak decoding accuracy and corresponding p-value of Bonferroni-significant voxels are listed separately for total brain matter, lesion matter and normal-appearing brain tissue (NABT). P-values are calculated using the Pearson's χ^2 test. Additionally, the total number of Bonferroni-significant voxels and the proportion of Bonferroni-significant voxels with respect to all voxels in the particular analysis are shown.

and thus this type of analysis depends on a priori hypotheses about disease-underlying structures. However, this limitation can be overcome by using a so-called searchlight approach (Haynes et al., 2007; Kriegeskorte et al., 2006) which searches across the whole volume for local patterns informative about the disease status (Hackmack et al., 2012; Weygandt et al., 2011). Voxel-wise analysis and ROI analysis, however, have the disadvantage to neglect connectivity patterns or interrelations that might exist among measurements of distinct voxels or brain regions, which have been shown to be relevant for disease classification in some cases (Bassett et al., 2008; He et al., 2008; Raj et al., 2010). Another major drawback of all three types of analyses is that they are biased to specific scales, namely the sampling rate of the data, and therefore disregard potential sources of variability in patients given by different scales.

By using wavelets to extract information on different spatial scales, we overcome this limitation and allow for a scale-dependent analysis. The major benefit of using the dual-tree complex wavelet transform for calculating the wavelet coefficients is its additional orientation selectivity. By this, we introduced a new representation of brain structure by defining features as a function of scale, orientation and location. In our analyses, we covered scales ranging from $[4 \text{ mm}]^3$ in scale I to $[128 \text{ mm}]^3$ in scale VI. Within each scale, data of 28 orientation subbands containing a varying number of locations (from 64^3 in scale I to 2^3 in scale VI) were extracted. We are not aware of any other clinical study using this rich source of information as a basis for disease classification.

Nevertheless, wavelets have advanced to a popular and powerful instrument to analyze biomedical or neuroimaging data (Akay, 1997; Bullmore et al., 2004; Laine, 2000; Sajda et al., 2002; Unser and Aldroubi, 1996; Van De Ville et al., 2006). For functional MRI, main applications include spatiotemporal resampling as a non-

parametric test of functional connectivity (Breakspear et al., 2004; Bullmore et al., 2004), time-series modeling in the wavelet domain (Maxim et al., 2005), inter-subject registration (Suckling et al., 2006) and multiresolution hypothesis testing (Fadili and Bullmore, 2004; Van De Ville et al., 2006). In structural MRI, wavelets have mostly been used to characterize texture in normal and abnormal tissue such as temporal lobes affected by epilepsy (Jafari-Khouzani et al., 2010), brain tumors (Sasikala and Kumaravel, 2008) or MS lesions (Harrison et al., 2010; Zhang et al., 2008, 2009). For reviews of texture analysis based on medical images, see Castellano et al. (2004), Kassner and Thornhill (2010) or Sajda et al. (2002). Additionally, wavelets have been used for image denoising (Laine, 2000), tissue segmentation (Barra and Boire, 2000), image registration (Dinov et al., 2002) or feature reduction (Lao et al., 2004). To the best of our knowledge, there is only one other study which used a combination of wavelets and SVMs for the purpose of diagnosing a disease: based on 2-dimensional MR images, Chaplot et al. (2006) used directly the wavelet coefficients of a particular scale as input to a SVM in order to classify between patients suffering from Alzheimer's disease and healthy controls.

A limitation of the present study is the missing link to the histopathology accounting for high decoding accuracies. Since TIRM images are relatively unspecific with respect to underlying MS pathology (Neema et al., 2007), analyzing possible pathomechanisms would require either histological data (e.g. from post-mortem brains) or advanced imaging data such as diffusion or magnetization transfer imaging data. In particular, the interpretation of directional information is challenging. Further studies are necessary to correlate histopathological findings or findings of non-conventional MRI with decoding accuracy as a function of scale, orientation and eventually location.

Conclusions

In conclusion, based on a combination of wavelets and pattern recognition methods, we identified a new class of features taking simultaneously scale and directionality information into account. These features were shown to contain substantial disease-relevant information for decoding MS and thus can be considered as 'disease signatures'. Since MRI interpretation is highly variable when relying on visual perception (Kassner and Thornhill, 2010; Klöppel et al., 2008a), diagnoses based on computerized techniques have the potential to be more reliable than diagnoses made by clinicians who might have different levels of training. Therefore, we think that our proposed features have a high potential to assist in the diagnostic process complementing macrotexture information already used by neuroradiologists. However, our approach is not limited to clinical applications in structural MRI, but might be also interesting for functional MRI studies investigating cognitive functions in healthy or diseased subjects.

Disclosure statement

The authors report no disclosures or potential conflicts of interest.

Acknowledgments

This work was supported by the Bernstein Computational Program of the German Federal Ministry of Education and Research (01GQ1001C, 01GQ0851, GRK 1589/1) and the German Research Foundation (Exc 257).

Appendix A. Supplementary data

Supplementary data to this article can be found online at <http://dx.doi.org/10.1016/j.neuroimage.2012.05.022>.

Histogram of decoding accuracies

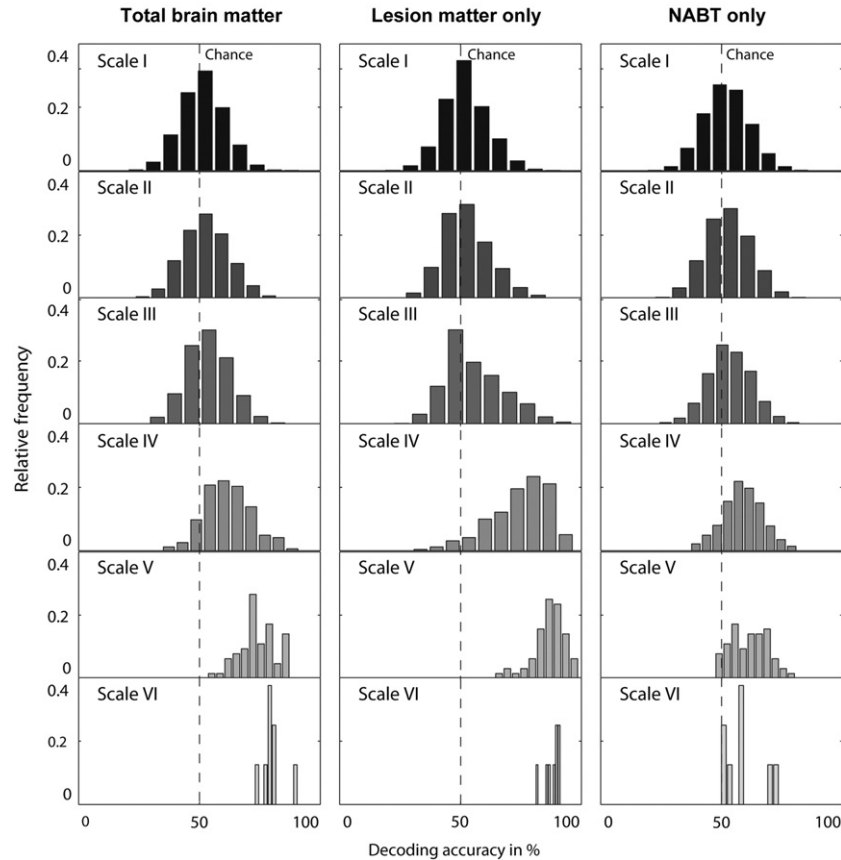


Fig. 6. Results of the local analysis of anisotropy II. Here, we show the relative distribution of scale-dependent decoding accuracies, separately for total brain matter, lesion matter and normal-appearing brain tissue (NABT). For each scale, the decoding accuracies were grouped into 10 equally spaced bins and corresponding frequencies were divided by the total number of classification analyses per scale.

References

- Akay, M., 1997. *Time Frequency and Wavelets in Biomedical Signal Processing* (IEEE Press Series on Biomedical Engineering). Wiley-IEEE Press.
- Antel, S.B., Collins, D.L., Bernasconi, N., Andermann, F., Shighal, R., Kearney, R.E., Arnold, D.L., Bernasconi, A., 2003. Automated detection of focal cortical dysplasia lesions using computational models of their MRI characteristics and texture analysis. *NeuroImage* 19, 1748–1759.
- Ashburner, J., Friston, K.J., 2000. Voxel-based morphometry – the methods. *NeuroImage* 11, 805–821.
- Ashburner, J., Friston, K.J., 2005. Unified segmentation. *NeuroImage* 26, 839–851.
- Ashburner, J., Klöppel, S., 2011. Multivariate models of inter-subject anatomical variability. *NeuroImage* 56, 422–439.
- Barra, V., Boire, J.Y., 2000. Tissue segmentation of MR images of the brain by possibilistic clustering on a 3D wavelet representation. *J. Magn. Reson. Imaging* 11, 267–278.
- Bassett, D.S., Bullmore, E., Verchinski, B.A., Mattay, V.S., Weinberger, D.R., Meyer-Lindenberg, A., 2008. Hierarchical organization of human cortical networks in health and schizophrenia. *J. Neurosci.* 28, 9239–9248.
- Bullmore, E., Fadili, J., Maxim, V., Sendur, L., Whitcher, B., Suckling, J., Brammer, M., Breakspear, M., 2004. Wavelets and functional magnetic resonance imaging of the human brain. *NeuroImage* 23 (Suppl 1), S234–S249.
- Burges, C.J.C., 1998. A tutorial on support vector machines for pattern recognition. *Data Min. Knowl. Disc.* 2, 121–167.
- Burrus, C.S., Gopinath, R.A., Guo, H., 1997. *Introduction to Wavelets and Wavelet Transforms: a Primer*. Prentice Hall.
- Castellano, G., Bonilha, L., Li, L.M., Cendes, F., 2004. Texture analysis of medical images. *Clin. Radiol.* 59, 1061–1069.
- Chang, C.C., Lin, C.J., 2011. LIBSVM: a library for support vector machines. *ACM Trans. Intell. Syst. Technol.* 2, 27:1–27:27. Software available at, <http://www.csie.ntu.edu.tw/~cjlin/libsvm/>.
- Chaplot, S., Patnaik, L.M., Jagannathan, N.R., 2006. Classification of magnetic resonance brain images using wavelets as input to support vector machine and neural network. *Biomed. Signal Process. Contr.* 1, 86–92.
- Compston, A., Coles, A., 2008. Multiple sclerosis. *Lancet* 372, 1502–1517.
- Cortes, C., Vapnik, V., 1995. Support-vector networks. *Mach. Learn.* 20, 273–297.
- Cutter, G.R., Baier, M.L., Rudick, R.A., Cookfair, D.L., Fischer, J.S., Petkau, J., Syndulko, K., Weisenker, B.G., Antel, J.P., Confavreux, C., Ellison, G.W., Lublin, F., Miller, A.E., Rao, S.M., Reingold, S., Thompson, A., Willoughby, E., 1999. Development of a multiple sclerosis functional composite as a clinical trial outcome measure. *Brain* 122, 871–882.
- Daubechies, I., 1988. Orthonormal bases of compactly supported wavelets. *Commun. Pure Appl. Math.* 41, 906–966.
- Daubechies, I., 1992. *Ten Lectures on Wavelets*. Society for Industrial and Applied Mathematics.
- Davatzikos, C., Resnick, S.M., Wu, X., Parmpi, P., Clark, C.M., 2008. Individual patient diagnosis of AD and FTD via high-dimensional pattern classification of MRI. *NeuroImage* 41, 1220–1227.
- Dinov, I.D., Mega, M.S., Thompson, P.M., Woods, R.P., Sumners, D.L., Sowell, E.L., Toga, A.W., 2002. Quantitative comparison and analysis of brain image registration using frequency-adaptive wavelet shrinkage. *IEEE Trans. Inf. Technol. Biomed.* 6, 73–85.
- Draganski, B., Martino, D., Cavanna, A.E., Hutton, C., Orth, M., Robertson, M.M., Critchley, H.D., Frackowiak, R.S., 2010. Multispectral brain morphometry in Tourette syndrome persisting into adulthood. *Brain* 133, 3661–3675.
- Du, A.T., Schuff, N., Kramer, J.H., Rosen, H.J., Gorno-Tempini, M.L., Rankin, K., Miller, B.L., Weiner, M.W., 2007. Different regional patterns of cortical thinning in Alzheimer's disease and frontotemporal dementia. *Brain* 130, 1159–1166.
- Ecker, C., Marquand, A., Mourão-Miranda, J., Johnston, P., Daly, E.M., Brammer, M.J., Maltezos, S., Murphy, C.M., Robertson, D., Williams, S.C., Murphy, D.G., 2010. Describing the brain in autism in five dimensions – magnetic resonance imaging-assisted diagnosis of autism spectrum disorder using a multiparameter classification approach. *J. Neurosci.* 30, 10612–10623.
- Fadili, M.J., Bullmore, E.T., 2004. A comparative evaluation of wavelet-based methods for hypothesis testing of brain activation maps. *NeuroImage* 23, 1112–1128.
- Filippi, M., Rocca, M.A., 2005. MRI evidence for multiple sclerosis as a diffuse disease of the central nervous system. *J. Neurol.* 252, S16–S24.
- Filippi, M., Rocca, M.A., 2010. Dirty-appearing white matter: a disregarded entity in multiple sclerosis. *AJNR Am. J. Neuroradiol.* 31, 390–391.
- Filippi, M., Comi, G., Rovaris, M., 2004. *Normal-appearing White and Grey Matter Damage in Multiple Sclerosis*. Springer, Berlin.
- Fu, C.H., Mourão-Miranda, J., Costafreda, S.G., Khanna, A., Marquand, A.F., Williams, S.C., Brammer, M.J., 2008. Pattern classification of sad facial processing: toward the development of neurobiological markers in depression. *Biol. Psychiatry* 63, 656–662.
- Ge, Y., Grossman, R.L., Babb, J.S., He, J., Mannon, L.J., 2003. Dirty-appearing white matter in multiple sclerosis: volumetric MR imaging and magnetization transfer ratio histogram analysis. *AJNR Am. J. Neuroradiol.* 24, 1935–1940.

- Graps, A., 1995. An introduction to wavelets. *Comput. Sci. Eng.* 2, 50–61.
- Hackmack, K., Weygandt, M., Wuerfel, J., Pfueller, C.F., Bellmann-Strobl, J., Paul, F., Haynes, J.D., 2012. Can we overcome the clinico-radiological paradox in multiple sclerosis? *J. Neurol.* Mar 24 (Electronic publication ahead of print).
- Harrison, L.C., Raunio, M., Holli, K.K., Luukkaala, T., Savio, S., Elovaara, I., Soimakallio, S., Eskola, H.J., Dastidar, P., 2010. MRI texture analysis in multiple sclerosis: toward a clinical analysis protocol. *Acad. Radiol.* 17, 696–707.
- Haynes, J.D., Rees, G., 2006. Decoding mental states from brain activity in humans. *Nat. Rev. Neurosci.* 7, 523–534.
- Haynes, J.D., Sakai, K., Rees, G., Gilbert, S., Frith, C., Passingham, R.E., 2007. Reading hidden intentions in the human brain. *Curr. Biol.* 17, 323–328.
- He, Y., Chen, Z., Evans, A., 2008. Structural insights into aberrant topological patterns of large-scale cortical networks in Alzheimer's disease. *J. Neurosci.* 28, 4756–4766.
- Jafari-Khouzani, K., Elisevich, K., Patel, S., Smith, B., Soltanian-Zadeh, H., 2010. FLAIR signal and texture analysis for lateralizing mesial temporal lobe epilepsy. *NeuroImage* 49, 1559–1571.
- Kassner, A., Thornhill, R.E., 2010. Texture analysis: a review of neurologic MR imaging applications. *AJNR* 31, 809–816.
- Kingsbury, N.G., 2000. A dual-tree complex wavelet transform with improved orthogonality and symmetry properties. *Proc. IEEE Int. Conf. Image Proc., Canada*, 2, pp. 375–378.
- Kingsbury, N.G., 2001. Complex wavelets for shift invariant analysis and filtering of signals. *Appl. Comput. Harmon. Anal.* 10, 234–253.
- Klöppel, S., Stonnington, C.M., Barnes, J., Chen, F., Chu, C., Good, C.D., Mader, I., Mitchell, L.A., Patel, A.C., Roberts, C.C., Fox, N.C., Jack Jr., C.R., Ashburner, J., Frackowiak, R.S., 2008a. Accuracy of dementia diagnosis: a direct comparison between radiologists and a computerized method. *Brain* 131, 2969–2974.
- Klöppel, S., Stonnington, C.M., Chu, C., Draganski, B., Scahill, R.I., Rohrer, J.D., Fox, N.C., Jack Jr., C.R., Ashburner, J., Frackowiak, R.S., 2008b. Automatic classification of MR scans in Alzheimer's disease. *Brain* 131, 681–689.
- Klöppel, S., Chu, C., Tan, G.C., Draganski, B., Johnson, H., Paulsen, J.S., Kienzle, W., Tabrizi, S.J., Ashburner, J., Frackowiak, R.S., 2009. PREDICT-HD Investigators of the Huntington Study Group. Automatic detection of preclinical neurodegeneration: presymptomatic Huntington disease. *Neurology* 72, 426–431.
- Koutsouleris, N., Meisenzahl, E.M., Davatzikos, C., Bottlender, R., Frodl, T., Scheuerecker, J., Schmitt, G., Zetsche, T., Decker, P., Reiser, M., Möller, H.J., Gaser, C., 2009. Use of neuroanatomical pattern classification to identify subjects in at-risk mental states of psychosis and predict disease transition. *Arch. Gen. Psychiatry* 66, 700–712.
- Kriegeskorte, N., Goebel, R., Bandettini, P., 2006. Information-based functional brain mapping. *Proc. Natl. Acad. Sci. U. S. A.* 103, 3863–3868.
- Kurtzke, J.F., 1983. Rating neurologic impairment in multiple sclerosis: an expanded disability status scale (EDSS). *Neurology* 33, 1444–1452.
- Laine, A.F., 2000. Wavelets in temporal and spatial processing of biomedical images. *Annu. Rev. Biomed. Eng.* 2, 511–550.
- Lao, Z., Shen, D., Yue, Z., Karaceli, B., Resnick, S.M., Davatzikos, C., 2004. Morphological classification of brains via high-dimensional shape transformations and machine learning methods. *NeuroImage* 21, 46–57.
- Loizou, C.P., Murray, V., Pattichis, M.S., Seimenis, I., Pantziaris, M., Pattichis, C.S., 2011. Multiscale amplitude-modulation frequency-modulation (AM-FM) texture analysis of multiple sclerosis in brain MRI images. *IEEE Trans. Inf. Technol. Biomed.* 15, 119–129.
- Mallat, S.G., 1989. A theory for multiresolution signal decomposition: the wavelet representation. *IEEE Trans. Pattern Anal. Mach. Intell.* 11, 674–693.
- Mallat, S., 2008. *A Wavelet Tour of Signal Processing*. Academic Press.
- Maxim, V., Sendur, L., Fails, J., Suckling, J., Gould, R., Howard, R., Bullmore, E., 2005. Fractional Gaussian noise, functional MRI and Alzheimer's disease. *NeuroImage* 25, 141–158.
- McDonald, W.I., Compston, A., Edan, G., Goodkin, D., Hartung, H.P., Lublin, F.D., McFarland, H.F., Paty, D.W., Polman, C.H., Reingold, S.C., Sandberg-Wollheim, M., Sibley, W., Thompson, A., van den Noort, S., Weinshenker, B.Y., Wolinsky, J.S., 2001. Recommended diagnostic criteria for multiple sclerosis: guidelines from the International Panel on the diagnosis of multiple sclerosis. *Ann. Neurol.* 50, 121–127.
- Meyer, Y., 1987. *Wavelets with Compact Support*. Zygmund Lectures, U. Chicago.
- Morgen, K., Sammer, G., Courtney, S.M., Wolters, T., Melchior, H., Blecker, C.R., Oschmann, P., Kaps, M., Vaitl, D., 2007. Distinct mechanisms of altered brain activation in patients with multiple sclerosis. *NeuroImage* 37, 937–946.
- Mur, M., Bandettini, P.A., Kriegeskorte, N., 2009. Revealing representational content with pattern-information fMRI – an introductory guide. *Soc. Cogn. Affect. Neurosci.* 4, 101–109.
- Neema, M., Stankiewicz, J., Arora, A., Dandamudi, V.S., Batt, C.E., Guss, Z.D., Al-Sabbagh, A., Bakshi, R., 2007. T1- and T2-based MRI measures of diffuse gray matter and white matter damage in patients with multiple sclerosis. *J. Neuroimaging* 17, 165–215.
- Nichols, T., Hayasaka, S., 2003. Controlling the familywise error rate in functional neuroimaging: a comparative review. *Stat. Methods Med. Res.* 12, 410–446.
- Oliveira Jr., P.P., Nitrini, R., Busatto, G., Buchpiguel, C., Sato, J.R., Amaro Jr., E., 2010. Use of SVM methods with surface-based cortical and volumetric subcortical measurements to detect Alzheimer's disease. *J. Alzheimers Dis.* 19, 1263–1272.
- Pujol, J., Soriano-Mas, C., Alonso, P., Cardoner, N., Mechón, J.M., Deus, J., Vallejo, J., 2004. Mapping structural brain alterations in obsessive-compulsive disorder. *Arch. Gen. Psychiatry* 61, 720–730.
- Raj, A., Mueller, S.G., Young, K., Laxer, K.D., Weiner, M., 2010. Network-level analysis of cortical thickness of the epileptic brain. *NeuroImage* 52, 1302–1313.
- Sailer, M., Fischl, B., Salat, D., Tempelmann, C., Schönfeld, M.A., Busa, E., Bodammer, N., Heinze, H.J., Dale, A., 2003. Focal thinning of the cerebral cortex in multiple sclerosis. *Brain* 126, 1734–1744.
- Sajda, P., Lane, A., Zeevi, Y., 2002. Multi-resolution and wavelet representations for identifying signatures of disease. *Dis. Markers* 18, 339–363.
- Sasikala, M., Kumaravel, N., 2008. A wavelet-based optimal texture feature set for classification of brain tumors. *J. Med. Eng. Technol.* 32, 198–205.
- Schölkopf, B., Smola, A.J., 2002. *Learning with Kernels*. MIT Press.
- Selesnick, I.W., Baraniuk, R.G., Kingsbury, N.G., 2005. The dual-tree complex wavelet transform. *IEEE Signal Process. Mag.* 22, 123–151.
- Shawe-Taylor, J., Christianini, N., 2000. *Support Vector Machines and Other Kernel-based Learning Methods*. Cambridge University Press.
- Sowell, E.R., Kan, E., Yoshii, J., Thompson, P.M., Bansal, R., Xu, D., Toga, A.W., Peterson, B.S., 2008. Thinning of sensorimotor cortices in children with Tourette syndrome. *Nat. Neurosci.* 11, 637–639.
- Suckling, J., Long, C., Triantafyllou, C., Brammer, M., Bullmore, E., 2006. Variable precision registration via wavelets: optimal spatial scales for inter-subject registration of functional MRI. *NeuroImage* 15, 197–208.
- Unser, M., Aldroubi, A., 1996. A review of wavelets in biomedical applications. *Proc. IEEE* 84, 626–638.
- Van De Ville, D., Blu, T., Unser, M., 2006. Surfing the brain: an overview of wavelet-based techniques for fMRI data analysis. *IEEE Eng. Med. Biol. Mag.* 25, 65–78.
- Vrenken, H., Seewann, A., Knol, D.L., Polman, C.H., Barkhof, F., Geurts, J.J., 2010. Diffusely abnormal white matter in progressive multiple sclerosis: in vivo quantitative MR imaging characterization and comparison between disease types. *AJNR Am. J. Neuroradiol.* 31, 541–548.
- Weygandt, M., Hackmack, K., Pfüller, C., Bellmann-Strobl, J., Paul, F., Zipp, F., Haynes, J.D., 2011. MRI pattern recognition in multiple sclerosis normal-appearing brain areas. *PLoS One* 6, e21138.
- Worbe, Y., Gerardin, E., Hartmann, A., Valabrégue, R., Chupin, M., Tremblay, L., Vidailhet, M., Colliot, O., Lehericy, S., 2010. Distinct structural changes underpin clinical phenotypes in patients with Gilles de la Tourette syndrome. *Brain* 133, 3649–3660.
- Yotter, R.A., Nenadic, I., Ziegler, G., Thompson, P.M., Gaser, C., 2011. Local cortical surface complexity maps from spherical harmonic reconstructions. *NeuroImage* 56, 961–973.
- Zhang, Y., Wells, J., Buist, R., et al., 2006. A novel MRI texture analysis of demyelination and inflammation in relapsing-remitting experimental allergic encephalomyelitis. *Med. Image Comput. Comput. Assist. Interv.* 9, 760–767.
- Zhang, J., Tong, L., Wang, L., Li, N., 2008. Texture analysis of multiple sclerosis: a comparative study. *Magn. Reson. Imaging* 26, 1160–1166.
- Zhang, Y., Zhu, H., Mitchell, J.R., et al., 2009. T2 MRI texture analysis is a sensitive measure of tissue injury and recovery resulting from acute inflammatory lesions in multiple sclerosis. *NeuroImage* 47, 107–111.

WEB REFERENCES

- SPM5 software (Wellcome Trust Centre for Neuroimaging, Institute of Neurology, UCL, London): <http://www.fil.ion.ucl.ac.uk/spm/>; last time accessed: November 4th 2011.
- Wavelet software (Electrical and Computer Engineering Polytechnic University, New York): <http://taco.poly.edu/WaveletSoftware/>; last time accessed: November 4th 2011.
- LIBSVM software (Department of Computer Science, National Taiwan University, Taiwan): <http://www.csie.ntu.edu.tw/~cjlin/libsvm/>; last time accessed: November 4th 2011.